

-Supplementary Information-

## Holographic Microscope Slide in Spatio-Temporal Imaging Modality for Reliable 3D Cell Counting

Biagio Mandracchia,<sup>a,\*‡</sup> Vittorio Bianco,<sup>a,‡</sup> Zhe Wang,<sup>a,b</sup> Martina Mugnano,<sup>a</sup> Alessia Bramanti,<sup>a,c</sup> Melania Paturzo,<sup>a</sup> and Pietro Ferraro.<sup>a</sup>

<sup>a</sup> Institute of Applied Sciences and Intelligent Systems—Italian National Research Council (ISASI-CNR), Via Campi Flegrei 34, 80078 Pozzuoli (NA), Italy.

<sup>b</sup> College of Applied Sciences, Beijing University of Technology, Beijing 100124, China.

<sup>c</sup> IRCCS Centro Neurolesi “Bonino Pulejo”, Messina, Italy.

\*Corresponding author: [b.mandracchia@isasi.cnr.it](mailto:b.mandracchia@isasi.cnr.it)

‡These authors equally contributed to the present work.

The throughput of cell counting in microfluidics is obviously related to the maximum flow rate of the sample through the channels. This can be augmented by increasing the speed of the sample and, then, the acquisition speed, or enlarging the volume in which the count is effectively performed. This last option is generally limited by the optical components available and the level of resolution required. Holographic imaging, on the other hand, gives the possibility to recover out-of-focus objects and to track accurately their position in the third dimension. The combination of these two features is very important for cell counting and density measurements because it allows the detection of otherwise overlooked objects, while retaining an accurate estimation of the volume actually scanned.

### Cell counting for STDH holograms

In STDH, the detection accuracy is strongly related to the synchronization between acquisition frame rate and velocity of the sample. In the ideal scenario, the flow control is perfect and the velocity of the sample inside the inspected volume is constant. In this case, the quality of STDH images is equivalent to standard off-axis holograms. However, if we want to perform the cell counting over the extended depth of field provided of STDH or if the flow rate is not stable, it is very likely that we face a distribution of velocities in the sample. In this case, not all the object are equally well sampled and useful information could be lost if we just relied on standard thresholding algorithms.

We have designed a specific decision algorithm for STDH holograms to improve the method robustness against not ideal flow conditions. This was conceived taking into account that: a) data are recorded using the STDH method and stored into an hybrid pitch synthetic hologram; b) Cells can be considered well sampled only if their velocity matches the CCD acquisition speed; c) we have *a priori* information about the sample, i.e. we know that a suspended RBC is spherically shaped when this is well sampled. Under these three

conditions described above, the following algorithm can automatically count cells flowing in the microfluidic channel and imaged by a STDH system.

In the microfluidic channel, even though a constant pressure is applied, the cells are expected to flow at different velocities, depending on their distance from the borders. In STDH, which is a volumetric counting method, it is important to count also the cells closer to the borders in order to take full advantage of the extended the depth of field. On the other hand, the shape of a cell in the STDH representation varies depending on its velocity. In other words, undersampled and oversampled cells will be represented as ellipses with various eccentricity factors on the hologram plane. Hence, classical thresholding of the sharp spots after propagating the hologram could not be the most reliable strategy to count them and a different approach needs to be followed.

Before describing our algorithm in details, it is worth emphasizing that:

- not only cells on the hologram plane but also cells on the other planes can be counted by numerical propagation;
- Although the cells' diffraction patterns overlap, the algorithm can locate each cell accurately.

The adopted counting algorithm is based on “Image Correlation Identification”. A thresholding algorithm can fail when dealing with overlapping cells of different shapes. In this case, a correct estimation of the number of cells can be hindered by the fact that different diffraction patterns are intersecting with each other. The creation of sample library helps sorting out these issues.

By choosing the proper model samples, we found that the error due to double counting can be reduced down to the 3%. We follow a “Recognize-Locate-Cover” (RLC) process that can be divided in three steps: i) the correlation recognition is used to find the approximate cell areas; ii) thresholding and image recognition algorithms are used to find the centroid position and filter out the real cells regions; iii) the entire dataset is scanned to check if all cells have been detected, in which case the process is terminated. In the main paper, we have tested the algorithm with RBCs.

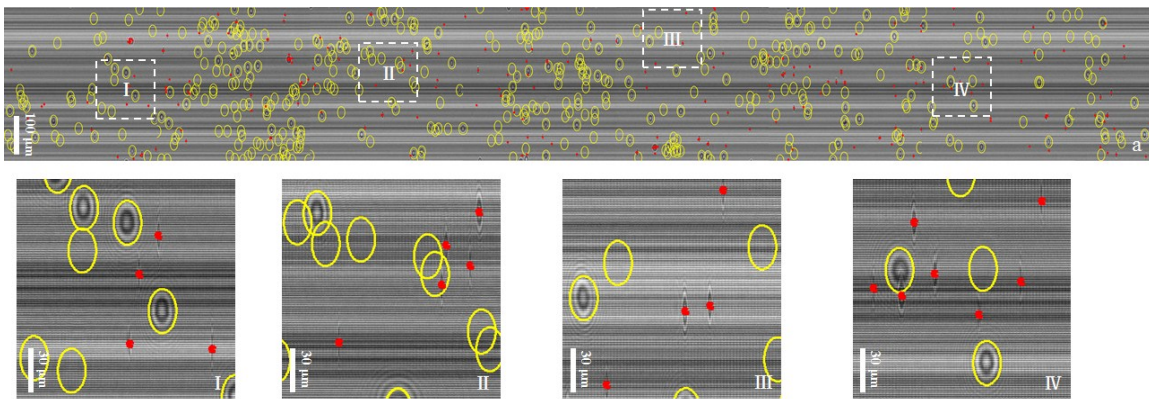


Fig. S1 Under-sampled and well-sampled cells detected on a portion of the acquired STDH; the yellow circles mark out the well-sampled cells and red dot mark out the under-sampled cells.

We can see from Fig. S1 that undersampled cells (red dots) are a small part of the total cell count, where well-sampled cells represent the majority (circled in yellow). Nonetheless, these can be an impairing source of error, especially if one wants to perform high-throughput volumetric imaging, as in the case of STDH.

To assess the advantage of volumetric imaging by holographic propagation, the counting algorithm was applied to both propagated and non-propagated data. In both cases, the RLC process is used to identify the cells, but with different sample libraries. Furthermore, counting the RBCs in the propagation planes requires an additional process of “double check”.

The basis of the STDH counting algorithm is the creation of a “sample library”. To create this library, we individuated a set of typical cell-shapes from a previously acquired dataset. To perform the counting on the hologram plane, the algorithm has been trained in order to identify six typical cell-shapes (see Fig. S2).

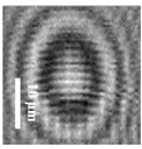
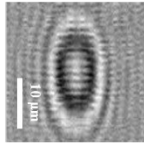
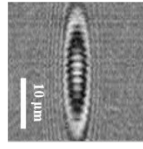
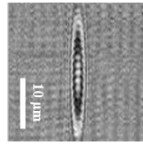
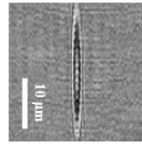
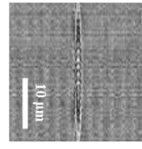
Sampling	Well-sampled RBC		Under-sampled RBC			
Type	Type 1	Type 2	Type 3	Type 4	Type 5	Type 6
Pattern						
Velocity	$v_1 = 83 \mu\text{m/s}$	$v_2 = 110 \mu\text{m/s}$	$v_3 = 231 \mu\text{m/s}$	$v_4 = 416 \mu\text{m/s}$	$v_5 = 520 \mu\text{m/s}$	$v_6 = 1040 \mu\text{m/s}$

Fig. S2: Six types of RBC in sample library of synthetic hologram.

### Non-volumetric cell counting

Cell shapes numbered from one to six represent the cells with different velocities; type 1 and type 2 are the well-sampled cells, while type 3-6 are under-sampled cells. After repeated testing and inspection, this sample library ensures a proper cell counting in the central area of the hologram plane.

A possible source of error is due to the presence of cells at the borders that are mostly outside of the field of view.

The cell-counting algorithm on the hologram plane can be divided into six steps:

1. Load a synthetic hologram  $H_0$  obtained from one of the chosen lines of the whole datasets.
2. Remove the background noise to create the clean hologram  $H_{nb}$ .
3. Select one cell type from the sample library to run the correlation identification.
4. Determine the centroid location of each cell. This is done by using thresholds and region proof algorithms. At the end of this step, all the cells centroids are stored the image  $H_{cr}$ .

5. Cover in  $H_{nb}$  a proper area around the newly found cell locations to avoid double counting. Size and shape of the covering areas depend on the specific cell type. The output is stored in  $H_c$ .
6. Repeat operations from 3 to 5 for each cell type in the library, using  $H_c$  as target image instead of  $H_{nb}$ .

The flow chart in Fig. S3 shows the details of the counting algorithm for the hologram plane.

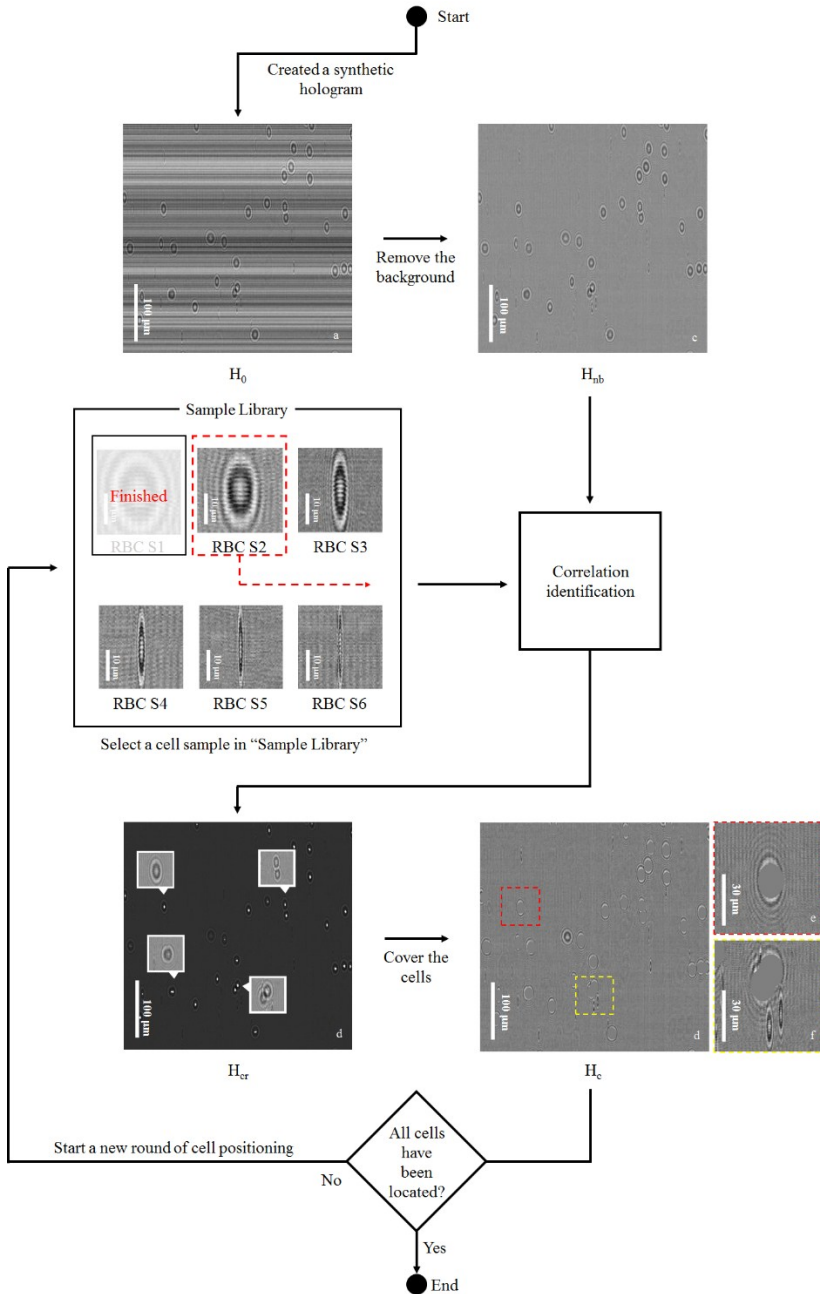


Fig. S3: The flow chart diagram for RLC processing the STDH. A small portion of the STDH is shown here for clarity.

In the hologram plane the sample library is formed by six cell shapes. In Fig. S4(a-f) we have indicated the centroids of the cells of each type with dots of different colors. Figure S4(g) shows the final output of counting algorithm on hologram plane. In Fig. S4(g) I-IV we can notice that partially overlapping cells are well counted: the different types of cells can be distinguished even if their diffraction pattern spatially overlap. This method was applied to three synthetic holograms of the same sample recorded by three different rows. The same cells pass through the field of view of all the three rows, thus the three corresponding synthetic holograms can be seen as three different measurements of the same sample. The final result of the non-holographic counting is  $7453 \pm 135$  cells.

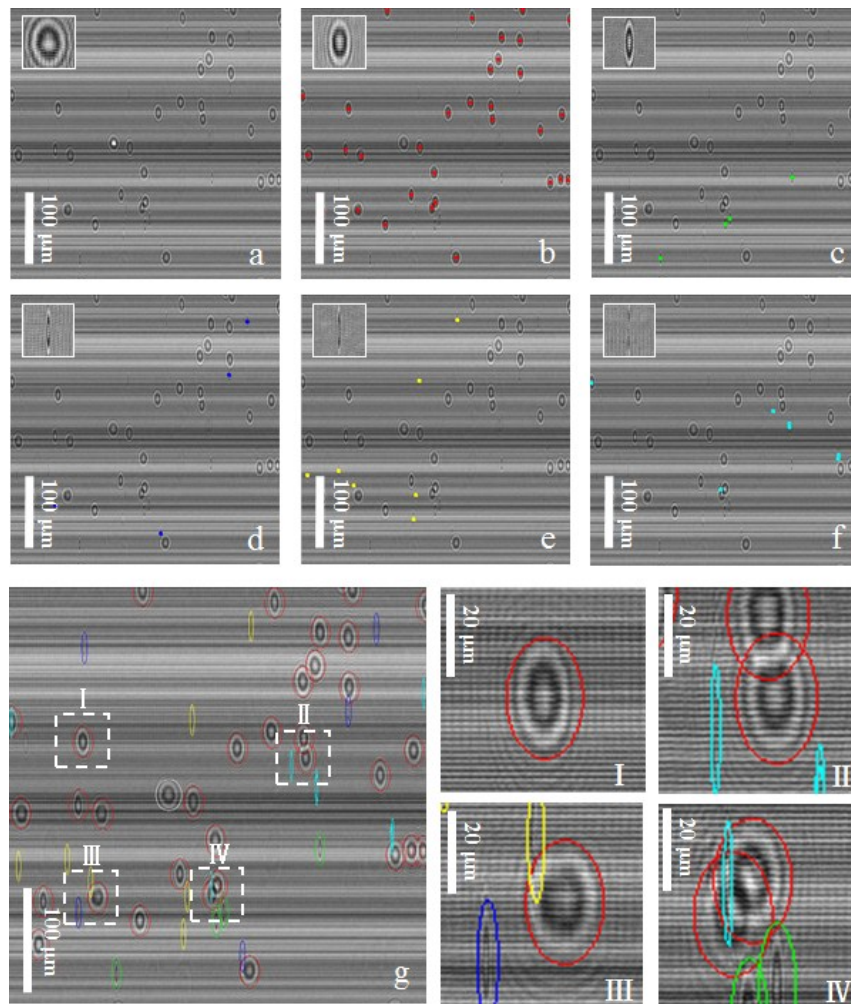


Fig. S4: Shape identification on the hologram plane. (a) - (f) Independent identification of cell types from 1 to 6 on the same portion of the hologram. (g) Final result of the identification algorithm. (I-IV) Zoomed sections showing different degrees of overlapping between the flowing RBCs.

## **Volumetric cell-counting**

Holographic reconstructions allow for a more accurate cell location along the z-axis, which is an essential feature for volumetric cell counting purposes. However fast cells can be under-sampled, leading to a low Signal-to-Noise Ratio (SNR) in the reconstruction phase and, in turn, to a cell miscounting.

The cell counting performed on holographic reconstructions after propagation is mostly similar to the aforementioned algorithm adopted for the hologram plane.

We performed the count on the same three holograms used in the previous case: the result of the counting is  $13156 \pm 40$ .

It is worth noting that the result is twice the number obtained with the non-holographic counting, while the error is less than one third.

## **Counting cells with Burker chamber hemocytometer**

Counting chambers serve to determine the number of particles per volume unit of a liquid. The particles (e.g., cells, leucocytes, erythrocytes, thrombocytes, bacteria, fungus spores, pollen) are visually counted under an inverted microscope. The microscope-slide-sized base plate is made of special optical glass.

Milled grooves divide the surface into two large fields (outside) and three narrow ridges (inside). The two outer fields are for inscriptions, whereas the ridges are ground and polished. The central ridge (= chamber bottom) has two engraved sets of rulings for counting, separated by a groove.

Generally the chamber bottom on the central ridge is 0.1 mm lower (= chamber depth) than the two outer ridges. Hence, when a cover glass is placed on top, there is a gap of 0.1 mm between the glass and the central ridge. The lateral boundaries of the volume to be counted are formed by the imaginary planes projected vertically onto the boundary lines of the ruling.

Burker chamber was used for cell counting. The ruling shows 9 large squares of 1 mm<sup>2</sup> each (Fig.S5a). These are used for counting red blood cells. Each large square is subdivided by double lines (0.05 mm apart) into 16 group squares with 0.2 mm sides (Fig.S5b).

The double lines form mini squares with an area of 0.0025 mm<sup>2</sup>. At least three squares delimited by triple lines are counted and each square corresponds to 1/10 mm<sup>3</sup>. An arithmetic average of counted cells is carried out. Then, the average is multiplied for dilution factor equal to 10.000.

Equation for particle determination:

Number of cells/ml volume: (average of three squares) \* 10000

In the large square shown in the Fig.S6 are counted 75 cells, in the other 2 large square 40 cells and 35 cells are counted. For cell determination the average of counting cells is carried out and it is equal to 50. Then, the average is multiplied for dilution factor equal to 10.000.

Final cell density was 500000 cells/ml.

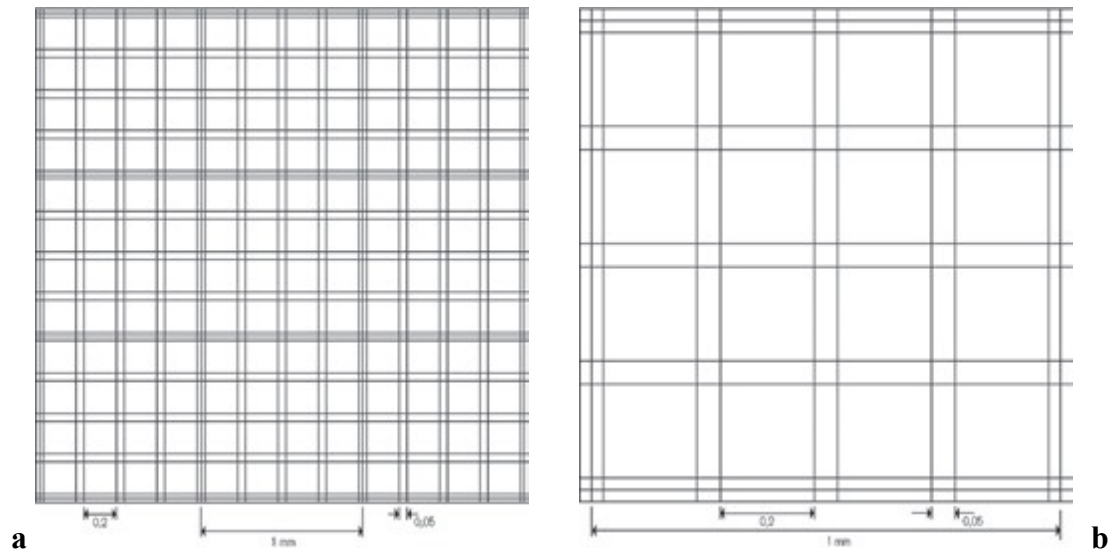


Figure S5: a) Burker chamber. b) Large central square.

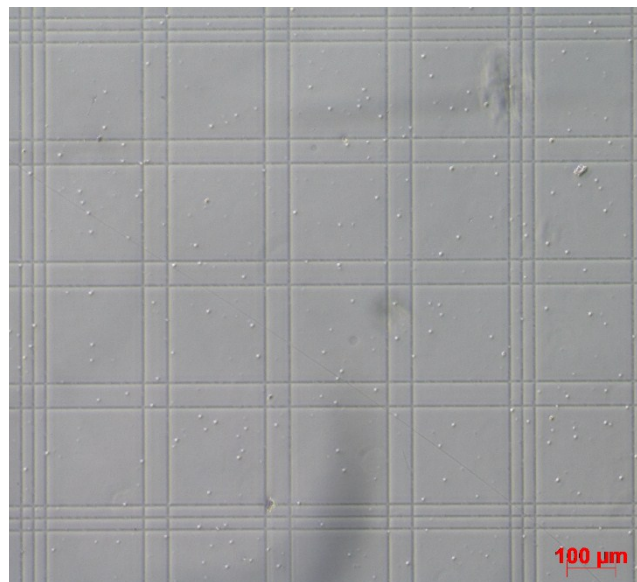


Figure S6: Burker chamber for RBCs counting. The image shows one of the three squares used to evaluate cell density.

## Estimation of cell Velocity

In this manuscript, we performed the counting and tracking of red blood cells using a line scan sensor. Assuming that RBCs' diffraction pattern is circular, we can estimate velocity from the stretching of the undersampled cells. In fact, we can measure the cell size along the spatial direction,  $d = N_y \cdot \Delta y / M$ , and the time it took to cover such distance along the temporal direction,  $t = N_t / F_R$ . The resulting velocity is:

$$v = \frac{d}{t} = \frac{N_y}{N_t} \cdot \frac{\Delta y \cdot F_R}{M}$$

Where  $N_y$  is the number of pixels along the spatial direction,  $N_t$  the number of pixels along the temporal direction,  $\Delta y$  the pixel size,  $M$  the magnification, and  $F_R$  the frame rate.